Ultrasonic Spray Coating for the ***scalable fabrication*** of Perovskite-on-Chalcogenide Monolithic Tandem Devices: Approaching the 20% Efficiency

Joao Silvano[123], Gizem Birant[123], Tim Oris[13], Jan D'Haen[12], Wim Deferme[12], Bart Vermang[123]**

[1]Imec − Partner in Solliance, Kapeldreef 75, 3000 Leuven, Belgium; [2]Hasselt University, Institute for Materials Research, Wetenschapspark 1, 3590 Diepenbeek, Belgium; [3]EnergyVille, Thor Park 8320, 3600 Genk, Belgium.

Corresponding Authors

*Prof. Dr. Bart Vermang; Email: bart.vermang@uhasselt.be

*Dr. Gizem Birant; Email: gizem.birant@imec.be

The combination of perovskite and chalcogenide solar cells allows for the monolithic fabrication of all-thin-film tandem with compositional tunability, facilitating optimal band gap alignment for an efficient absorption of the sunlight spectrum, while empowering flexible photovoltaic applications. However, this combination is yet to reach the levels of efficiency and production scalability seen in perovskite/silicon tandems, mostly due to the challenging fabrication of perovskite cells on top of the irregular chalcogenide cell surface. Herein, we propose to enhance the scalability of the technology by developing the ultrasonic spray coating of perovskite on top of Cu(In,Ga)S(Se) (CIGS) cells for the fabrication of monolithic tandem devices. The capability of the technique to deposit conformal perovskite coatings, aligned with interlayer optimization, results in the successful integration of perovskite and chalcogenide cells. The resulting monolithic tandem devices exhibit efficiencies close to 20%, a significant improvement on the efficiency of the single junction perovskite and CIGS reference cells. These results offer a promising pathway towards the upscaling of perovskite/CIGS device fabrication.

TOC GRAPHICS

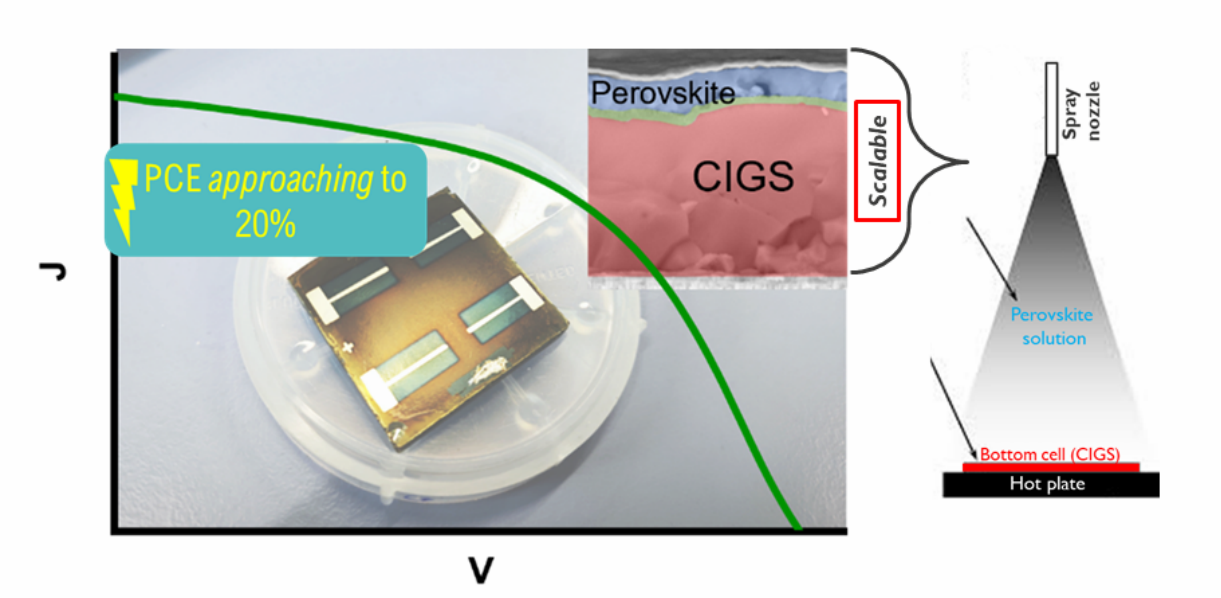
PCE approaching to 20%
Perovskite
CIGS
Scalable
Spray nozzle
Perovskite solution
Bottom cell (CIGS)
Hot plate
J
V

MAIN TEXT

The surge in global energy demand propelled by the trend for overall electrification calls for sustainable and efficient energy generation solutions. Solar power plays a key role in this electric future, and photovoltaic (PV) energy generation must grow accordingly. Considering spatial requirements and the cost distribution of a PV system, in which only about one third is associated with the price of the PV module[1], it is desirable to have solar cell technologies with higher efficiencies than the currently widespread silicon (Si) modules. Multijunction solar cells are regarded as the solution for this problem, combining two or more absorbing materials to surpass the Shockley-Queisser limit for single junction cells[2]. Among the available technologies, perovskite solar cells (PSCs) align efficiencies as high as 26%[3], low cost[4], and compositional flexibility, resulting in band gap tunability[5]. These advantages have caused many research groups worldwide to invest in the development of perovskite-based tandem devices, which has led to a rapid increase in efficiency, with perovskite/silicon tandems recently reaching 33.9% power conversion efficiency (PCE)[6].

Using silicon bottom cells, however, comes with some limitations. The production of crystalline silicon is an energy demanding process with a high carbon footprint, and the resulting device is rigid. Chalcogenide solar cells are a thin-film alternative, using significantly less material and offering a lightweight solution compatible with flexible applications[7]. While crystalline silicon has a much larger market penetration, CIGS solar cells are also established technologies with a significant market share[8] and have had their fabrication process continuously optimized for over 40 years[9]. In spite of that, the irregular morphology of the top surface of chalcogenide cells creates a challenge for the integration of a solution processed perovskite top cell for monolithic

tandems. This has slowed down the development of perovskite/CIGS tandem devices, which exhibit a record PCE of 24.2%[10], significantly lower than the record for perovskite/silicon tandems. Nevertheless, the technology shows promise, and studies have shown that with optimizations of the device this efficiency can be raised to 25%[11], or even approach the 30% mark[10,12].

On top of closing the efficiency gap, another crucial factor to bring perovskite/CIGS tandems towards commercialization is fabrication scalability. All champion efficiencies mentioned previously were obtained via spin coating of perovskite, a method that allows precise control of crystallization and uniform deposition in lab-scale, but is unsuitable for industrial or roll-to-roll manufacturing. Scalability of perovskite deposition has been the topic of many studies[13,14], and single junction solar cells have been successfully fabricated by scalable techniques, such as blade coating[15,16], slot die coating[17], and spray coating[18]. Yet, scalable deposition of perovskite on top of textured or rough bottom cells to fabricate monolithic tandem devices remains a challenge, with practical examples mostly focusing on perovskite/silicon tandems[19]. Fabricating perovskite/CIGS monolithic tandem devices requires a technique with the capability to deposit a conformal perovskite layer on a rough surface. Ultrasonic spray coating (USSC) makes use of an ultrasonic nozzle capable of transferring high frequency sound waves into a liquid to create standing waves, which causes the dispersion of the liquid into a fine mist of micron sized droplets[20]. By combining this nozzle with an air shaping system, it is possible to coat thin films of a functional ink onto a multitude of substrates, including rough surfaces. The technique has been used to produce high performance PSCs[21,22] and even deposit perovskite conformal layers on textured silicon[23].

In this study we propose the ultrasonic spray coating of perovskite to fabricate monolithic tandem devices with CIGS bottom cells. By adopting the same optimized deposition parameters used in the fabrication of perovskite single junction cells[24] (*i.e.*, deposition of perovskite on flat substrate, *kindly refer to Supporting Figure 1 for film quality*), we display the flexibility of USSC as a deposition technique for high quality perovskite layers, paving the way for its use in a multitude of applications. Scanning electron microscopy revealed a conformal coating of the interlayer and perovskite top cell with uniform thickness following the roughness of the CIGS bottom cells, and performance analysis indicate a nearly perfect sum of the two individual sub cells' open circuit voltages (V_{oc}) in the V_{oc} of the complete tandem device. The resulting monolithic perovskite/CIGS cell shows increased performance when compared with the individual cells, with a champion device PCE of 20.1%.

The design of the tandem stack considers the combination of a perovskite sub cell with bandgap of 1.6 eV ($Cs_{0.18}FA_{0.82}Pb(I_{0.94}Br_{0.06})_3$) with a CIGS bottom cell with bandgap of 1.0 eV, as optical simulations show this combination to be in the region of highest theoretical efficiency[25]. The stack, represented in **Figure 1**, also makes use of auxiliary layers in between the two absorbing materials. The CIGS cell, with a molybdenum (Mo)-based bottom electrode, operates with a cadmium sulfide (CdS) p-type buffer layer, additionally protecting the CIGS layer during the deposition of the window layer. The window layer is constituted of zinc-oxide (ZnO) and indium-tin-oxide (ITO). The first prevents the formation of shunt paths and short circuit between CIGS and ITO, while the ITO is used as a tunneling layer to connect the two sub cells and aids in current matching. The hole transport layer (HTL) of the perovskite cell is made of a nickel oxide (NiOx) and a self-assembled monolayer (SAM), with the latter being used for interface alignment with minimal non-radiative losses, ultimately enhancing the performance of PSCs[26,27].

A representative comparison between ultrasonically spray coated perovskite cells (single junction) with and without the SAM is shown in **Figure 2**. The monolayer generated a significant gain in V_{oc} for the cells processed with it, resulting in overall increased efficiency. The triple layer of lithium fluoride (LiF), buckminsterfullerene (C60), and bathocuproine (BCP) function as the electron transport layer, with LiF being a passivation layer and BCP a work function buffer layer. The top ITO and silver (Ag) layer constitute the top contact of the monolithic device. **Figure 3** is a representation of a processed sample (with 4 distinct tandem cells), including the exposed back contact (Mo) used during measurements. Additional details on the fabrication and device architecture can be found in the experimental methods section.

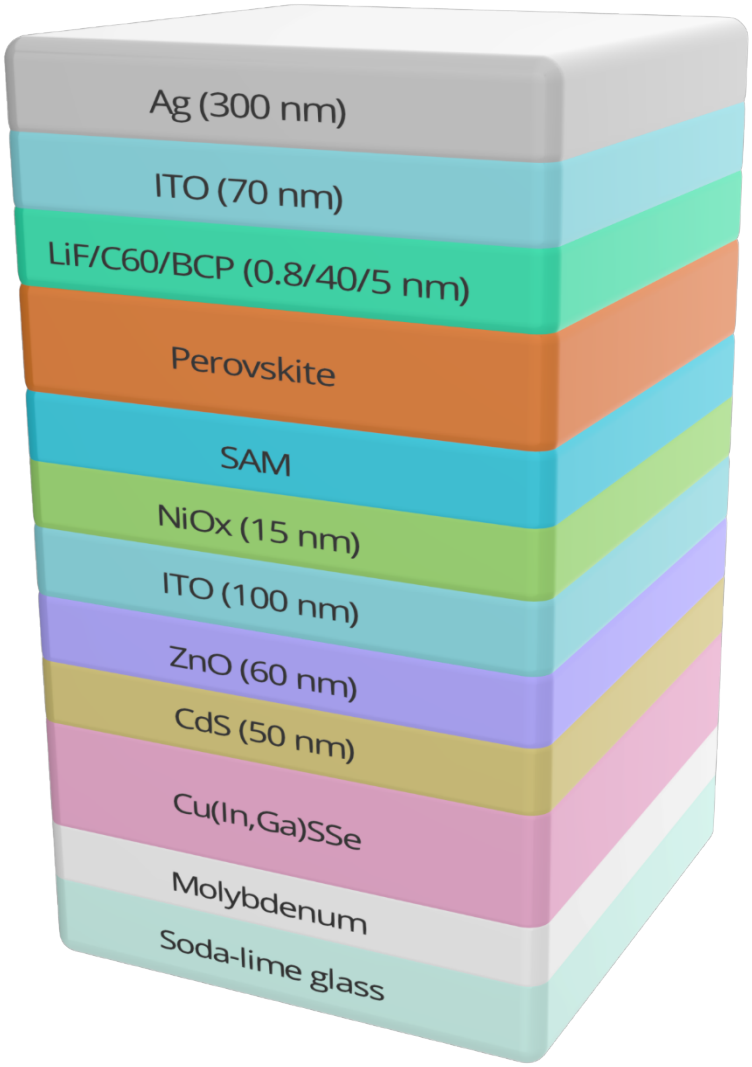

Figure 1. Representation of the tandem device stack, with CIGS bottom cell, interlayer, and perovskite top cell.

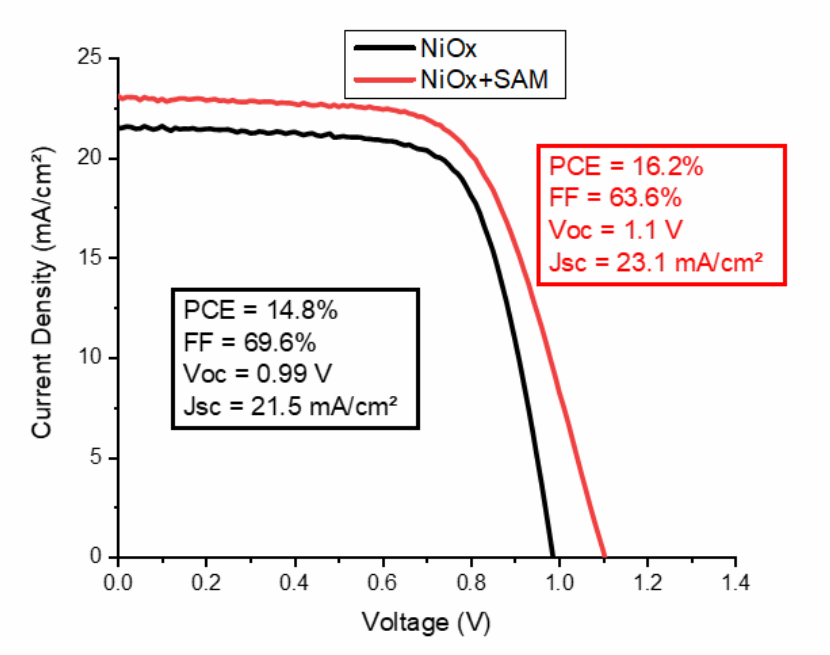

Figure 2. JV curves of single junction perovskite cells fabricated by ultrasonic spray coating, with and without the SAM.

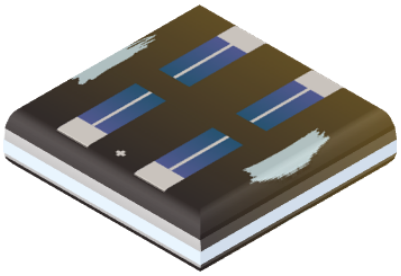

Figure 3. Schematic of a fabricated sample, with 4 distinct monolithic tandem devices.

Cross-section scanning electron microscopy (SEM) revealed that the layers on top of the bottom cell were successfully deposited as conformal films, following the roughness of the CIGS top surface (**Figure 4**). While this is expected for thermally evaporated materials, the perovskite solution deposition and crystallization can sometimes result in an irregular film, filling out the crevasses of the bottom layers while having a smooth top surface. This variation in thickness along the perovskite layer is detrimental to the operation of the solar cell, as it introduces

unbalanced absorption of light and interferes with current matching. Instead, when using ultrasonic spray coating as the deposition technique, microscopic droplets of the perovskite solution are uniformly dispersed along the surface of the substrate, resulting in a crystalline perovskite film of uniform thickness (around 300 nm). On top of that, the SEM images also reveal the presence of localized structural defects on the bottom side of the perovskite film, where it interfaces the HTL. Similar defects were also observed in single junction devices[24].

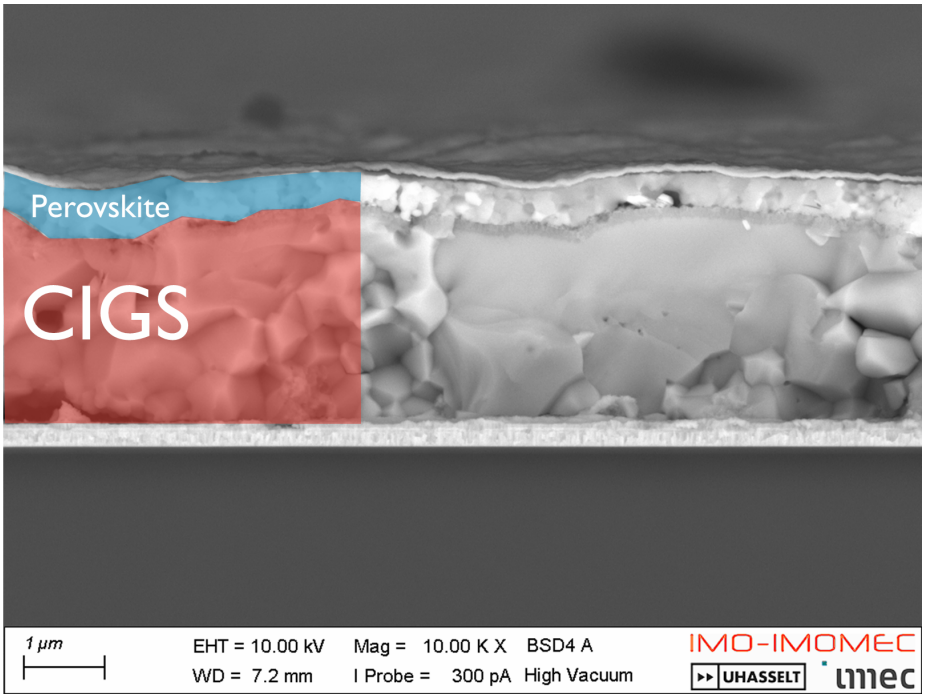

Figure 4. Cross-section SEM image of a monolithic tandem stack. The ultrasonically spray coated perovskite layer follows the roughness of the bottom CIGS cell.

The JV measurements of the produced tandem devices revealed an excellent V_{oc} in most cells, with the total V_{oc} of the tandem cell being close to the sum of the typical V_{oc} values of both sub cells (1.1 V for perovskite and 0.5 V for the CIGS, when operating as single junction cells). Out of the 22 working tandem devices produced, 12 exhibited V_{oc} above 1.5 V, with the average

value between all devices being 1.44 V. A higher variability was verified in device efficiency, with PCEs ranging from 5 to 20%. It is noteworthy that the variability is often seen when comparing cells within the same sample, with two cells on one side of the sample performing way above the opposite two, this could be due to the gas quenching step not affecting the entire 3x3 cm² area uniformly. The best performing cells indicate that the technique is able to produce high performing devices, with replicability relying on processing optimization, such as the use of an air knife for more uniform quenching. With that in mind, the 4 top performing cells (T-A, T-B, T-C, and T-D, all processed with the same parameters) are presented in **Figure 5** and **Table 1**.

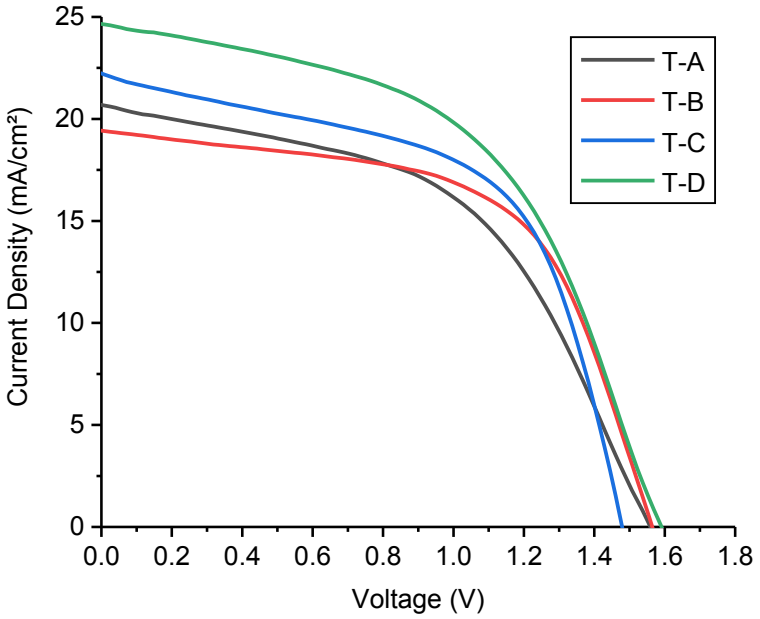

Figure 5. JV curves of four perovskite-on-CIGS monolithic tandem devices, fabricated by ultrasonic spray coating of the perovskite layer.

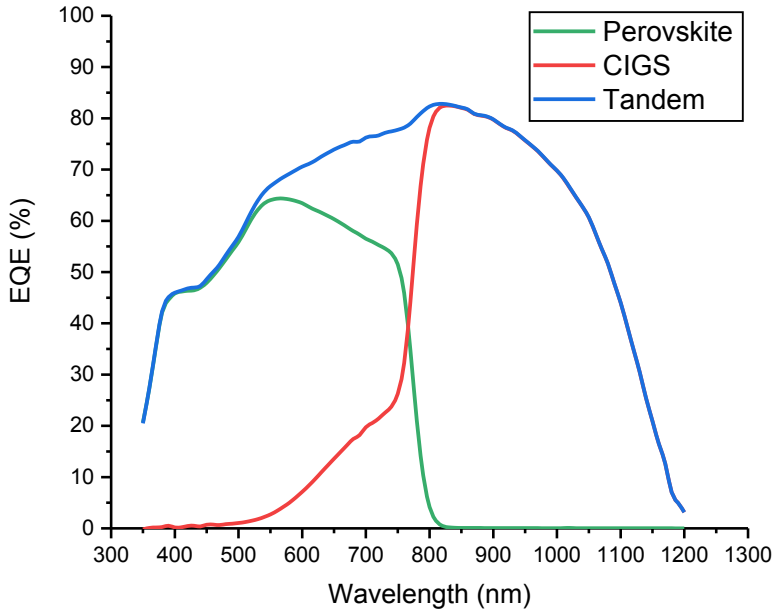

Figure 6. External quantum efficiency curve of a perovskite-on-CIGS monolithic tandem device.

Table 1. Device parameters extracted from JV measurements of four perovskite-on-CIGS monolithic tandem devices. Parameters of an ultrasonically spray coated perovskite single junction and a CIGS single junction reference cells produced for this study are presented for comparison. R_{Shunt} refers to shunt resistance, and R_{series} refers to series resistance.

Cell	**Jsc [mA/cm2]**	**Voc [V]**	**FF [%]**	**PCE [%]**	**R_{Shunt} [Ω*cm2]**	**R_{Series} [Ω*cm2]**
Perovskite (Single junction)	23.1	1.10	63.6	16.2	1262.6	13.3
CIGS (Single junction)	29.0	0.54	62.5	9.8	642.7	4.2
T-A	20.7	1.56	50.6	16.3	288.2	25.1
T-B	19.4	1.56	58.7	17.9	437.4	18.6
T-C	22.3	1.48	56.8	18.7	171.8	11.0

T-D	24.8	1.59	51.1	20.2	341.8	24.5

The 4 tandem cells have efficiencies superior to the spray coated perovskite single junction cell, although with a significant loss in fill factor. The larger area of the tandem devices (0.45 cm^2), when compared to the single junction perovskite cell (0.13 cm^2), can increase the odds of the cell to exhibit significant structural defects on the perovskite layer, which can lead to recombination of charges and electrical losses on the devices. The higher degree of shunting (lower R_{shunt}), when compared to the single junction cells, can lead to an overestimation of the J_{sc} due to a bending of the curve near the "J" axis, which is made apparent in the case of cell T-D. In this case, the determined J_{sc} (24.8 mA/cm^2) is higher than the J_{sc} of the limiting cell (23.1 mA/cm^2 for the perovskite top cell, when in single junction configuration). In our previous investigation concerning the ultrasonic spray coating of perovskite layers[24], a significant factor was identified as contributing to variability in sample quality and performance. This variability stems from the non-uniform and manual air quenching of the perovskite layer, primarily due to the use of an air gun focused on the center of the square sample. Without the spinning motion inherent in the spin coating process, which facilitates the even dispersion of the wet layer across the entire sample, this method results in a noticeable ring formation at the sample edges. Consequently, cells from different regions of a sample may exhibit varying characteristics. To address this challenge, adopting an automized quenching setup optimized for large areas, such as air knife gas quenching[28], plasma quenching[29], or flash infrared sintering[30], holds promise for enhancing reproducibility.

External quantum efficiency (EQE) measurements of the selected devices revealed semi-identical curves, with slight variation on the perovskite peak intensity (between 62 and 65%). The EQE of cell T-B is shown in **Figure 6**. The overall EQE of the perovskite top cell is below expected, based on the single junction optimization study[24]. The perovskite deposited in the monolithic device exhibits similar characteristics as to those obtained with non-optimal quenching, with a large step around the 400 nm region, corresponding to the interface between the perovskite and the HTL. It is noteworthy that the perovskite layer suffered increased exposure to air and humidity, due to the JV measurements being performed outside of the glovebox, which can cause degradation, especially in this interface region where defects are more present. This is further supported by the difference of the EQE-calculated short circuit current (14.7 mA/cm^2 for the perovskite curve and 16.7 mA/cm^2 for the CIGS curve) and the one measured in the solar simulator (19.4 mA/cm^2) with minimal exposure to air up to the time of measurement. On the other hand, the discrepancy of the currents between JV and EQE measurements might have been caused by shunts or current from outside the active area.

Overall, the ultrasonic spray coating of perovskite allowed the fabrication of monolithic tandem devices. The conformal nature of the perovskite layer, as revealed by SEM images, showcases the potential of this technique to effectively coat complex and rough substrates, such as the CIGS bottom cell. The investigation into device performance highlights the intricate challenges posed by the processing of tandem structures on rough surfaces, leading to variations in device efficiency. Furthermore, EQE measurements show that the interface between the perovskite and the hole transport layers can be optimized, aiming to avoid the formation of structural defects on the perovskite film. Nevertheless, the high performance exhibited by many of the fabricated

devices, with a high average value of V_{oc} and champion cell surpassing the 20% efficiency threshold with no anti-reflection coating, underscores the promising capabilities of ultrasonic spray coating in producing high-performance monolithic tandem devices. While addressing the replicability issue is essential for large scale production, these initial results firmly establish the foundation for further exploration of perovskite-on-CIGS monolithic fabrication.

EXPERIMENTAL METHODS

The perovskite solution is prepared as previously reported[24], considering the stoichiometric proportion of $Cs_{0.18}FA_{0.82}Pb(I_{0.94}Br_{0.06})_3$ to obtain a bandgap of 1.6 eV. The solvent used is a mixture of 15% N-methyl-2-pyrrolidone (NMP) and 85% dimethylformamide (DMF), in volume. The self-assembled monolayer is made of [4-(3,6-Dimethyl-9H-carbazol-9-yl)butyl]phosphonic Acid (Me-4PACz) (from TCI). The SAM ink is prepared by dissolving the Me-4PACz in Ethanol (99.5% extra dry, from AcroSeal), with concentration of 0.5 mM. The solution is mixed in ultrasonic bath for 30 min at room temperature before deposition. A solution of Al_2O_3 nanoparticles, used to improve the wettability of the SAM, is obtained by diluting 125 µL of Al_2O_3 nanoparticle solution (50 nm particle size, 20 wt% in isopropanol, from sigma aldrich), in 4.875 mL of 1-butanol (anhydrous, 99.8%, from sigma aldrich).

The fabrication of the tandem devices starts from a CIGS bottom cell obtained from AVANCIS, which is based on Mo-coated soda lime glass with alkali barrier, followed by the formation of CIGSSe absorber layer through annealing the Stacked Elemental Layer of Na-doped CuInGa with a Se-capping layer in a Rapid Thermal Annealing process in the presence of sulfur atmosphere. The CdS buffer layer is deposited by chemical bath. The ZnO, ITO tunneling layers, and the NiO_x are deposited by linear sputtering, using a Nebula linear sputtering system (from

Angstrom Engineering Inc.). The ITO deposition is done only in the cell areas, by using metallic masks. The NiO_x is annealed in air at 180 °C for 30 min. The SAM is deposited by ultrasonic spray coating (Impact nozzle, from Sono-Tek), with flow rate of 1.5 mL/min, hot plate temperature of 30 °C, path speed of 30 mm/sec, and N_2 pressure of 3 bar. The Al_2O_3 nanoparticles are deposited by dynamic spin-coating, with 3000 rpm rotation speed, and annealed inside the glovebox at 100 °C for 5 min. The perovskite ink is deposited by ultrasonic spray coating (Impact nozzle, from Sono-Tek), with flow rate of 1 mL/min, hot plate temperature of 40 °C, path speed of 30 mm/sec, and N_2 pressure of 3 bar. Gas quenching is performed with a N_2 airgun with pressure of 7.6 bar, 2 cm away from the substrate. The perovskite films are then annealed inside the glovebox at 100 °C for 30 min. The triple ETL is deposited by thermal evaporation (deposition tool from Angstrom Engineering Inc.). The top ITO electrode is deposited similarly to the tunneling layer, with the use of masks. Finally, the silver contact is deposited by thermal evaporation with an additional mask, creating the contact points and fingers illustrated in **Figure 3**. The molybdenum bottom contact is exposed by scratching the finished sample with a scalpel outside of the cell areas. The reference single junction perovskite cell was fabricated using a similar design as the top cell on the tandem stack, with the exception of the contacts: ITO is deposited on glass for the transparent bottom contact, and the top ITO and silver contact are replaced by copper, directly deposited on top of the ETL by thermal evaporation. The reference CIGS cell is fabricated similarly to the tandem devices up to the ZnO and ITO layers.

The cross-section SEM images were taken using a field-emission scanning electron microscope (Zeiss 450 FEG-SEM with Gemini 2 column). External quantum efficiency (EQE) measurements were made using a LOANA solar cell analysis system (from PV tools GmbH). The JV measurements of tandem and reference CIGS cells were obtained using a solar simulator

(ORIEL) with AM1.5 illumination at 25 °C. The JV measurements of single junction perovskite reference cells were obtained using a solar simulator (Abet Technology) with AM1.5 illumination at 25 °C inside a N_2-filled glovebox. In the fabrication of tandem devices all layers deposited after the NiO_x are deposited, treated, and stored inside a N_2-filled glovebox. The samples are exposed to air only right before the characterization methods, with exposure time of around 10 minutes for the ORIEL solar simulator and 30 minutes for the EQE measurements.

AUTHOR INFORMATION

Emails: bart.vermang@uhasselt.be; gizem.birant@uhasselt.be

https://www.imec-int.com/

https://www.uhasselt.be/imo

https://www.energyville.be/

Notes

The authors declare no competing financial interest.

ACKNOWLEDGMENT

This study was supported by the Special Research Fund (BOF) of Hasselt University, BOF number: BOF19OWB17. This project has also received funding from the European Union's Horizon 2020 research and innovation program under grant agreement No. 850937. G. Birant thanks Research Foundation Flanders FWO for the funding through the project number 1219423N. We would like to express our gratitude to AVANCIS for the partnership and for supplying the CIGS absorbers in this study.

REFERENCES

(1) Ramasamy, V.; Zuboy, J.; O'Shaughnessy, E.; Feldman, D.; Desai, J.; Woodhouse, M.; Basore, P.; Margolis, R. *U.S. Solar Photovoltaic System and Energy Storage Cost*

Benchmarks, With Minimum Sustainable Price Analysis: Q1 2022. National Renewable Energy Laboratory. NREL/TP-7A40-83586. Golden, CO, **2022**. https://www.nrel.gov/docs/fy22osti/83586.pdf (accessed 2023-08-08).

(2) Shockley, W.; Queisser, H. J. Detailed Balance Limit of Efficiency of p-n Junction Solar Cells. *J. Appl. Phys.* **1961**, *32* (3), 510-519. DOI: 10.1063/1.1736034

(3) Omrani, M.; Keshavarzi, R.; Abdi-Jalebi, M.; Gao, P. Impacts of plasmonic nanoparticles incorporation and interface energy alignment for highly efficient carbon-based perovskite solar cells. *Sci. Rep.* **2022** *12*, 5367. DOI: 10.1038/s41598-022-09284-9

(4) Li, Z.; Zhao, Y.; Wang, X.; Sun, Y.; Zhao, Z.; Li, Y.; Zhou, H.; Chen, Q. Cost Analysis of Perovskite Tandem Photovoltaics. *Joule* **2018**, *2* (8), 1559-1572. DOI: 1016/j.joule.2018.05.001

(5) Kulkarni, S. A.; Baikie, T.; Boix, P. P.; Yantara, N.; Mathews, N.; Mhaisalkar, S. Band-gap tuning of lead halide perovskites using a sequential deposition process. *J. Mater. Chem. A* **2014**, *2* (24), 9221-9225. DOI: 10.1039/C4TA00435C

(6) Green, M. A., Dunlop, E. D., Yoshita, M., Kopidakis, N., Bothe, K., Siefer, G., & Hao, X. Solar cell efficiency tables (Version 63). *Progress in Photovoltaics: Research and Applications* **2023,** 32 (1), 3-13. DOI: 10.1002/pip.3750

(7) Hamtaei, S.; Brammertz, G.; Poortmans, J.; Vermang, B. A review on barrier layers used in flexible stainless-steel based CIGS photovoltaic devices. *Npj Flex. Electron.* **2023**, *7*, 36. DOI: 10.1038/s41528-023-00266-z

(8) Philipps, S. *Photovoltaics Report.* Fraunhofer ISE and Werner Warmuth, PSE Projects GmbH. Freiburg, Germany, 2023

https://www.ise.fraunhofer.de/en/publications/studies/photovoltaics-report.html (accessed 2023-08-08).

(9) NREL Interactive Best Research-Cell Efficiency Chart. https://www.nrel.gov/pv/interactive-cell-efficiency.html (accessed 2023-08-08).

(10) Jošt, M.; Köhnen, E.; Al-Ashouri, A.; Bertram, T.; Tomšič, Š.; Magomedov, A.; Kasparavicius, E.; Kodalle, T.; Lipovšek, B.; Getautis, V.; Schlatmann, R.; Kaufmann, C. A.; Albrecht, S.; Topič, M. Perovskite/CIGS Tandem Solar Cells: From Certified 24.2% toward 30% and Beyond. *ACS Energy Lett.* **2022**, *7* (4), 1298–1307. DOI: 10.1021/acsenergylett.2c00274

(11) Ruiz-Preciado, M. A.; Gota, F.; Fassl, P.; Hossain, I. M.; Singh, R.; Laufer, F.; Schackmar, F.; Feeney, T.; Farag, A.; Allegro, I.; Hu, H.; Gharibzadeh, S.; Nejand, B. A.; Gevaerts, V. S.; Simor, M.; Bolt, P. J.; Paetzold, U. W. Monolithic Two-Terminal Perovskite/CIS Tandem Solar Cells with Efficiency Approaching 25%. *ACS Energy Lett.* **2022**, *7* (7), 2273–2281. DOI: 10.1021/acsenergylett.2c00707

(12) Shrivastav, N.; Kashyap, S.; Madan, J.; Al-Mousoi, A. K.; Mohammed, M. K. A.; Hossain, M. K.; Pandey, R.; Ramanujam, J. Perovskite-CIGS Monolithic Tandem Solar Cells with 29.7% Efficiency: A Numerical Study. *Energy Fuels* **2023**, *37* (4), 3083–3090. DOI: 10.1021/acs.energyfuels.2c03973

(13) Yang, F.; Jang, D.; Dong, L.; Qiu, S.; Distler, A.; Li, N.; Brabec, C. J.; Egelhaaf, H.-J. Upscaling Solution-Processed Perovskite Photovoltaics. *Adv. Energy Mater.* **2021**, *11*, 2101973. DOI: 10.1002/aenm.202101973

(14) Yang, Z.; Liu, Z.; Ahmadi, V.; Chen, W.; Qi, Y. Recent Progress on Metal Halide Perovskite Solar Minimodules. *Sol. RRL*. **2021**, *6*, 2100458. DOI: 10.1002/solr.202100458

(15) Wang, Z.; Zeng, L.; Zhang, C.; Lu, Y.; Qiu, S.; Wang, C.; Liu, C.; Pan, L.; Wu, S.; Hu, J.; Liang, G.; Fan, P.; Egelhaaf, H.-J.; Brabec, C. J.; Guo, F.; Mai, Y. Rational Interface Design and Morphology Control for Blade-Coating Efficient Flexible Perovskite Solar Cells with a Record Fill Factor of 81%. *Adv. Funct. Mater.* **2020**, *30*, 2001240. DOI: 10.1002/adfm.202001240

(16) Chen, S.; Xiao, X.; Gu, H.; Huang, J. Iodine reduction for reproducible and high-performance perovskite solar cells and modules. *Sci. Adv.* **2021**, *7* (10), eabe8130. DOI: 10.1126/sciadv.abe8130

(17) Di Giacomo, F.; Shanmugam, S.; Fledderus, H.; Bruijnaers, B. J.; Verhees, W. J. H.; Dorenkamper, M. S.; Veenstra, S. C.; Qiu, W.; Gehlhaar, R.; Merckx, T.; Aernouts, T.; Andriessen, R.; Galagan, Y. Up-scalable sheet-to-sheet production of high efficiency perovskite module and solar cells on 6-in. substrate using slot die coating. *Sol. Energy Mater. Sol. Cells.* **2018**, *181*, 53-59. DOI: 10.1016/j.solmat.2017.11.010

(18) Alanazi, T. I. Current spray-coating approaches to manufacture perovskite solar cells. *Results Phys.* **2023**, *44*, 106144. DOI: 10.1016/j.rinp.2022.106144

(19) Qiang, Z.; Wang, C.; Gao, X.; Zhao, X.; Tian, H.; Wang, W.; Zong, J.; Fan, J. Challenges of Scalable Development for Perovskite/Silicon Tandem Solar Cells. *ACS Appl. Energy Mater.* **2022**, *5* (6), 6499–6515. DOI: 10.1021/acsaem.2c00354

(20) Sono-tek. *How Ultrasonic Nozzles Work*. https://www.sono-tek.com/ultrasonic-coating/how-ultrasonic-nozzles-work/ (accessed 2023-08-08).

(21) Bishop, J. E.; Smith, J. A.; Lidzey, D. G. Development of Spray-Coated Perovskite Solar Cells. *ACS Appl. Mater. Interfaces*. **2020**, *12* (43), 48237–48245. DOI: 10.1021/acsami.0c14540

(22) Cassella, E. J.; Spooner, E. L. K.; Thornber, T.; O'Kane, M. E.; Catley, T. E.; Bishop, J. E.; Smith, J. A.; Game, O. S.; Lidzey, D. G. Gas-Assisted Spray Coating of Perovskite Solar Cells Incorporating Sprayed Self-Assembled Monolayers. *Adv. Sci.* **2022**, *9*, 2104848. DOI: 10.1002/advs.202104848

(23) Sansoni, S.; De Bastiani, M.; Aydin, E.; Ugur, E.; Isikgor, F. H.; Al-Zahrani, A.; Lamberti, F.; Laquai, F.; Meneghetti, M.; De Wolf, S. Eco-Friendly Spray Deposition of Perovskite Films on Macroscale Textured Surfaces. *Adv. Mater. Technol.* **2020**, *5*, 1901009. DOI: 10.1002/admt.201901009

(24) Silvano, J.; Hamtaei, S.; Verding, P.; Vermang, B.; Deferme, W. Investigating the Fabrication of Perovskite Solar Cells by Ultrasonic Spray Coating: A Design of Experiments Approach. *ACS Appl. Energy Mater.* **2023**, *6* (14), 7363–7376. DOI: 10.1021/acsaem.3c00491

(25) Feurer, T. Narrow band gap Cu(In,Ga)Se2 for tandem solar cell application. Ph.D. Dissertation, ETH Zurich, Zurich, Switzerland, 2019. https://www.research-collection.ethz.ch/handle/20.500.11850/389221 (accessed 2023-08-08).

(26) Magomedov, A.; Al-Ashouri, A.; Kasparavičius, E.; Strazdaite, S.; Niaura, G.; Jošt, M.; Malinauskas, T.; Albrecht, S.; Getautis, V. Self-Assembled Hole Transporting

Monolayer for Highly Efficient Perovskite Solar Cells. *Adv. Energy Mater.* **2018**, *8* (32), 1801892. DOI: 10.1002/aenm.201801892

(27) Al-Ashouri, A.; Magomedov, A.; Roß, M.; Jošt, M.; Talaikis, M.; Chistiakova, G.; Bertram, T.; Márquez, J. A.; Köhnen, E.; Kasparavičius, E.; Levcenco, S.; Gil-Escrig, L.; Hages, C. J.; Schlatmann, R.; Rech, B.; Malinauskas, T.; Unold, T.; Kaufmann, C. A.; Korte, L.; Niaura, G.; Getautis, V.; Albrecht, S. Conformal monolayer contacts with lossless interfaces for perovskite single junction and monolithic tandem solar cells. *Energy Environ. Sci.* **2019**, *12*, 3356-3369. DOI: 10.1039/C9EE02268F

(28) Cassella, E. J., Spooner, E. L. K., Thornber, T., O'Kane, M. E., Catley, T. E., Bishop, J. E., Smith, J. A., Game, O. S., & Lidzey, D. G. Gas Assisted Spray Coating of Perovskite Solar Cells Incorporating Sprayed Self Assembled Monolayers. *Adv. Sci.* **2022,** *9* (14). DOI: 10.1002/advs.202104848

(29) Rolston, N., Scheideler, W. J., Flick, A. C., Chen, J. P., Elmaraghi, H., Sleugh, A., Zhao, O., Woodhouse, M., & Dauskardt, R. H. Rapid Open-Air Fabrication of Perovskite Solar Modules. *Joule* **2020**, *4* (12), 2675–2692. DOI: 10.1016/j.joule.2020.11.001

(30) Sánchez, S., Vallés-Pelarda, M., Alberola-Borràs, J.-A., Vidal, R., Jerónimo-Rendón, J. J., Saliba, M., Boix, P. P., & Mora-Seró, I. Flash infrared annealing as a cost-effective and low environmental impact processing method for planar perovskite solar cells. *Mat. Today* **2019**, *31*, 39–46. DOI: 10.1016/j.mattod.2019.04.021

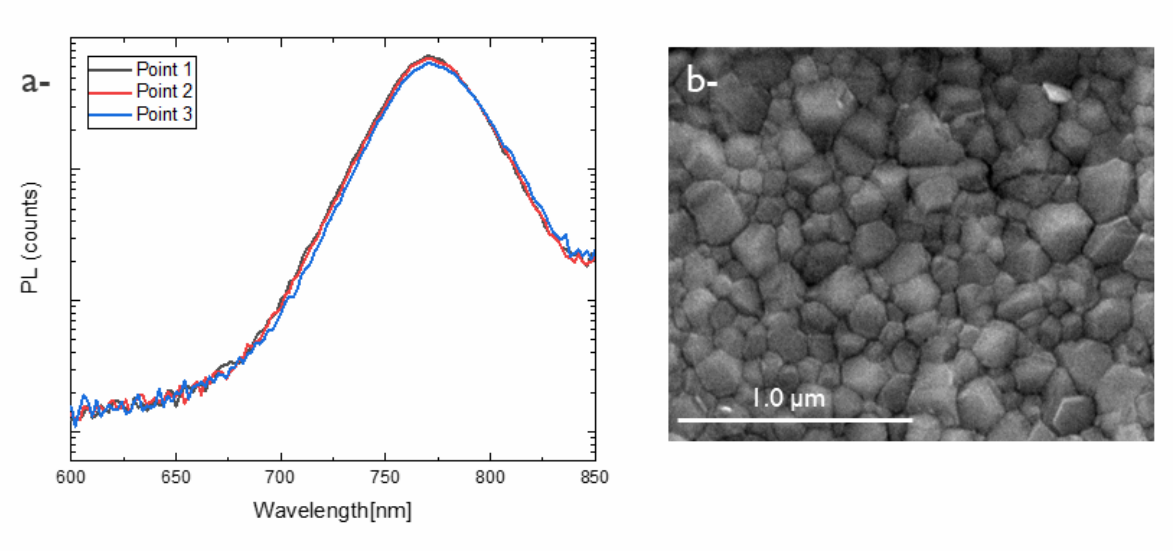

Supporting Figure 1: a- Photoluminescence response from three different regions and b- top-view scanning electron microscopy image, from fresh-spray coated perovskite film to show the quality of the film. The PL response indicates that the film quality can be slightly diverse depending on the sample region, but overall, the film has a homogenous response, i.e., a homogenous coating. The top-view SEM image indicates the small grains and closed-pack layer formation.